Electronic Supporting Information

Modular development of Metal Oxide / Carbon Composites for Electrochemical Energy Conversion and Storage

Yuanchun Ji,[†a,b] Yuan Ma,[†b,c] Rongji Liu,[a] Yanjiao Ma,[b,c] Kecheng Cao,[d] Ute Kaiser,[d] Alberto Varzi,[b,c] Yu-Fei Song,*[e] Stefano Passerini,*[b,c] and Carsten Streb*[a,b]

[a.] Institute of Inorganic Chemistry I, Ulm University, Albert-Einstein-Allee 11, D-89081 Ulm, Germany.

[b.] Helmholtz Institute Ulm (HIU), Helmholtzstrasse 11, D-89081 Ulm, Germany

[c.] Karlsruhe Institute of Technology (KIT), P.O. Box 3640, D-76021 Karlsruhe, Germany

[d.] Central Facility for Electron Microscopy, Group of Electron Microscopy of Materials Science, Ulm University, Albert-Einstein-Allee 11, D-89081 Ulm, Germany

[e.] Beijing Advanced Innovation Center for Soft Matter Science and Engineering, State Key Laboratory of Chemical Resource Engineering, Beijing University of Chemical Technology, Beijing, P. R. China.

Corresponding Authors

*Email: songyf@mail.buct.edu.cn;

*Email: stefano.passerini@kit.edu;

*Email: carsten.streb@uni-ulm.de

1. Instrumentation

High resolution scanning electron microscopy (HRSEM): The morphology and structure of all samples was investigated via field-emission scanning electron microscopy (SEM, ZEISS 1550VP). Samples were measured at 10 k eV acceleration voltage.

Transmission electron microscopy (TEM): TEM was performed on JEOL JEM-1300 under an accelerating voltage of 200 kV.

Aberration-corrected high-resolution electron microscopy (AC-HRTEM): High resolution transmission electron microscopy was carried out using a Cs-corrected FEI 80-300 TEM operated at 80 and 300 kV. The aqueous solution of the respective materials was drop-cast on holey carbon films and air-dried.

X-ray photoelectron spectroscopy (XPS): XPS measurements were performed using monochromatized Al Kα radiation on a PHI Quantera SXM system. Peak fitting was done with the CasaXPS software using Shirley background subtraction and mixed Gaussian-Lorentzian peak shapes.

FT-IR spectroscopy: FT-IR spectroscopy was performed on a Shimadzu FT-IR-8400S spectrometer. Samples were prepared as KBr pellets.

Thermogravimetric analysis (TGA): TGA was performed on a Setaram Setsys CS Evo, 30 - 800 °C at 10 K/min, 50 mL/min N_2, graphite crucible 0.5 mL.

Elemental Analysis was carried out on a CNH(S)-Analyser. Elementar Vario MICRO cube.

Cyclic Voltammetry (CV): CV measurements in oxygen evolution reaction were carried out on a CH Instruments CHI660E electrochemical workstation. And CV measurements in battery test

were carried in a VMP3 potentiostat (Bio-Logic Science Instruments), with the voltage range of 0.01-3.0 V.

Battery capacity and galvanostatic charging/discharging were measured on a Maccor 3000 battery tester, with the voltage range of 0.01-3.0 V.

Powder X-ray diffraction (Powder XRD) was collected on a Rigaku XRD-6000 diffractometer using Cu Kα radiation (λ = 0.154 nm).

N_2 sorption experiments were performed on an Quantachrome Autosorb-iQ. Data were analyzed using the Brunauer-Emmett-Teller (BET method).

General remarks: All chemicals were purchased from Sigma Aldrich, ABCR or VWR and were of reagent grade. The chemicals were used without further purification.

2. Characterization

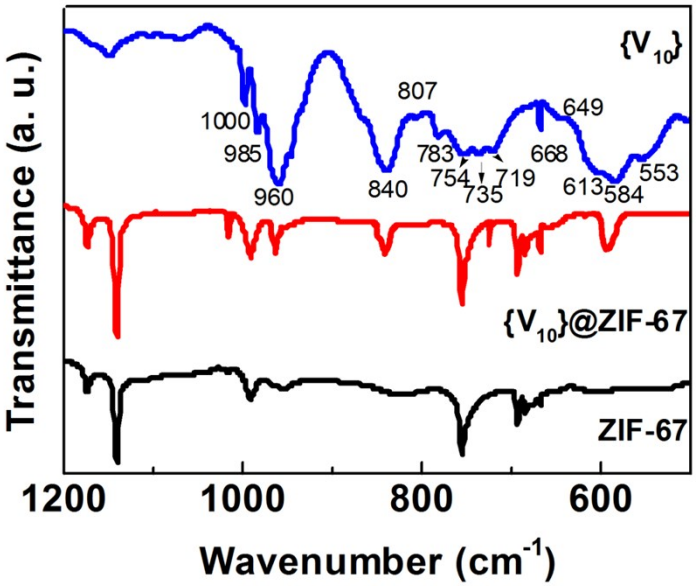

Figure S1. FT-IR spectra of $TBA_3\{V_{10}\}$, ZIF-67 and **$\{V_{10}\}$@ZIF-67**.

The characteristic signals of $TBA_3\{V_{10}\}$ are observed in the fingerprint region below 1000 cm^{-1}. The bridging symmetric and asymmetric vibrations of V-O-V are observed at 585, 730, and 840 cm^{-1}, respectively. The strong IR band at 960 cm^{-1} is assigned to V-$O_{terminal}$ stretching vibrations.[1–3]

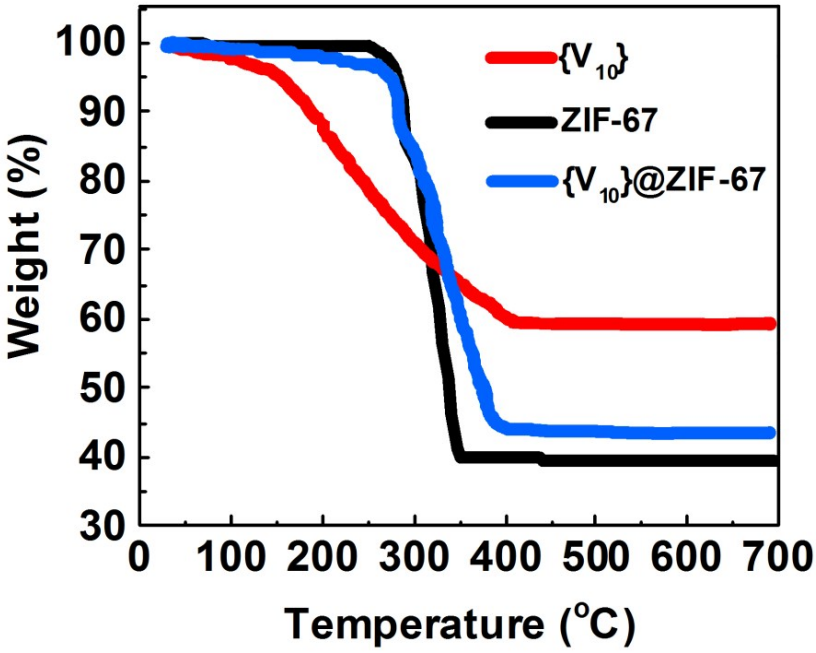

Figure S2 TGA curves of ZIF-67, $TBA_3\{V_{10}\}$ and $\{V_{10}\}$@ZIF-67. Condition: N_2 atmosphere, 10 °C/min, graphite crucible 0.5 mL.

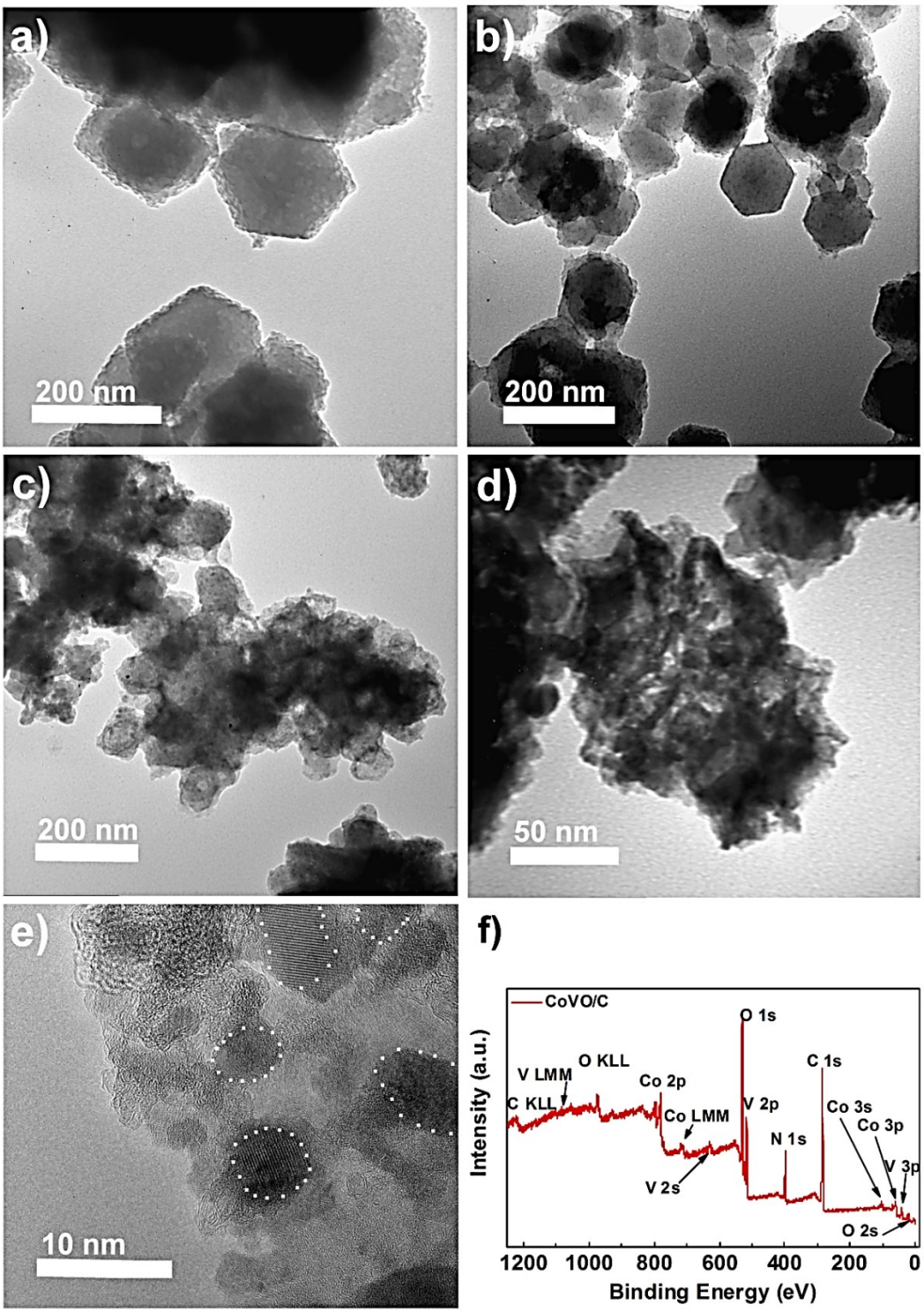

Figure S3. TEM images of a) pristine ZIF-67 pyrolyzed at 280 °C; b) **{V_{10}}@ZIF-67** pyrolyzed at 280 °C; c) **{V_{10}}@ZIF-67** pyrolyzed at 400 °C; HRTEM images of d), e) **CoVO/C** (**{V_{10}}@ZIF-67** pyrolyzed at 480 °C); and f) XPS survey spectrum of **CoVO/C**.

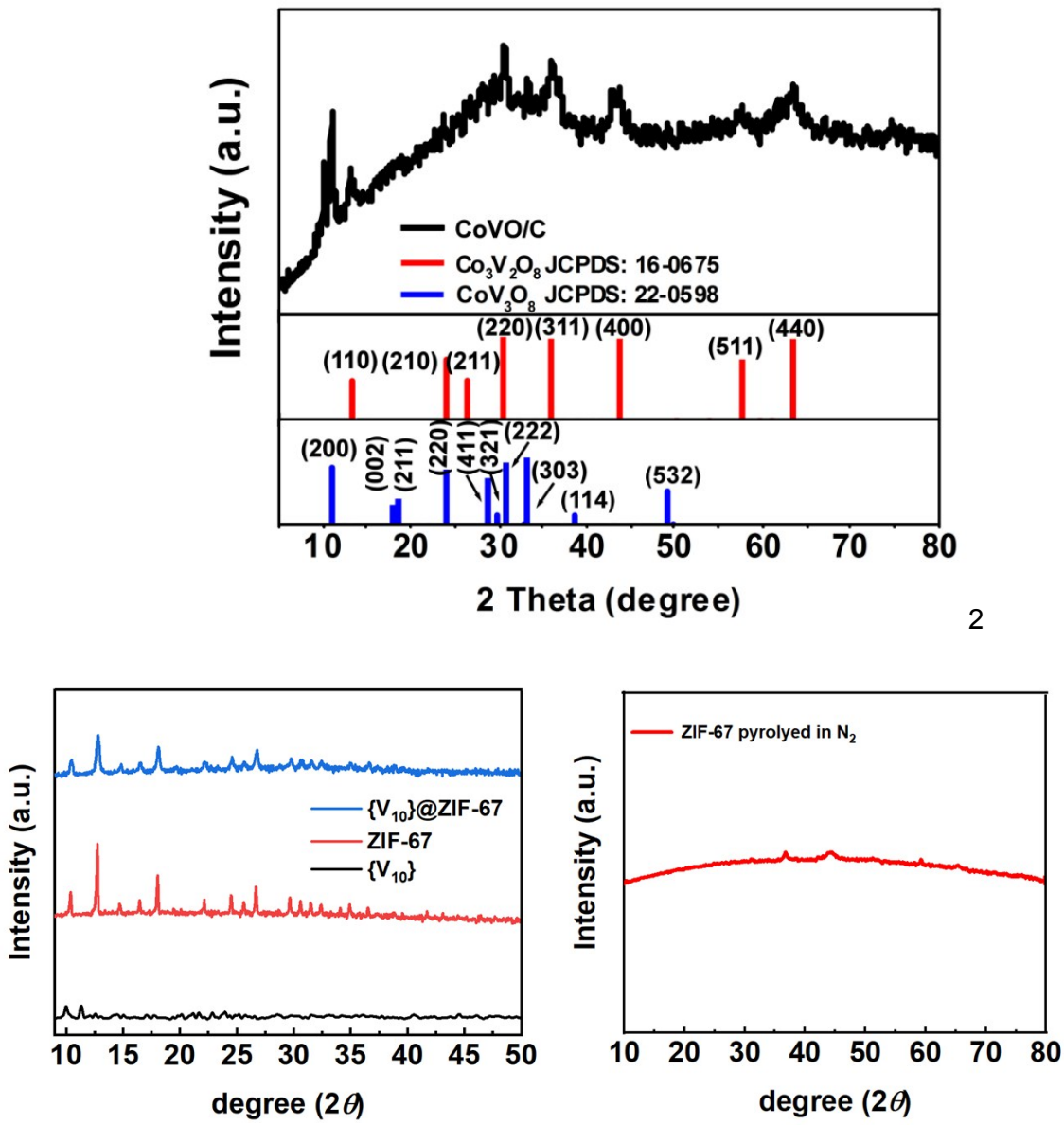

Figure S4. **Top:** Powder XRD pattern of **CoVO/C**. The database entries for $Co_3V_2O_8$ (JCPDS: 16-0675) and CoV_3O_8 (JCPDS: 22-0598) are shown in red and blue. Bottom left: powder XRD data for the reference materials. Bottom right: powder XRD data for native ZIF-67 pyrolyzed in N_2.

Powder XRD (pXRD) showed the presence of the two crystalline Co-V-oxide phases $Co_3V_2O_8$ (JCPDS card no. 16-0675) and CoV_3O_8 (JCPDS card no. 22-0598) in **CoVO/C** (Figure. S4). Specifically, the (110), (220), (311), (400), (511) and (440) lattice planes of $Co_3V_2O_8$ as well as the (200), (211), (411), (303), (114) and (532) planes of CoV_3O_8 match well with the experimental pXRD pattern.

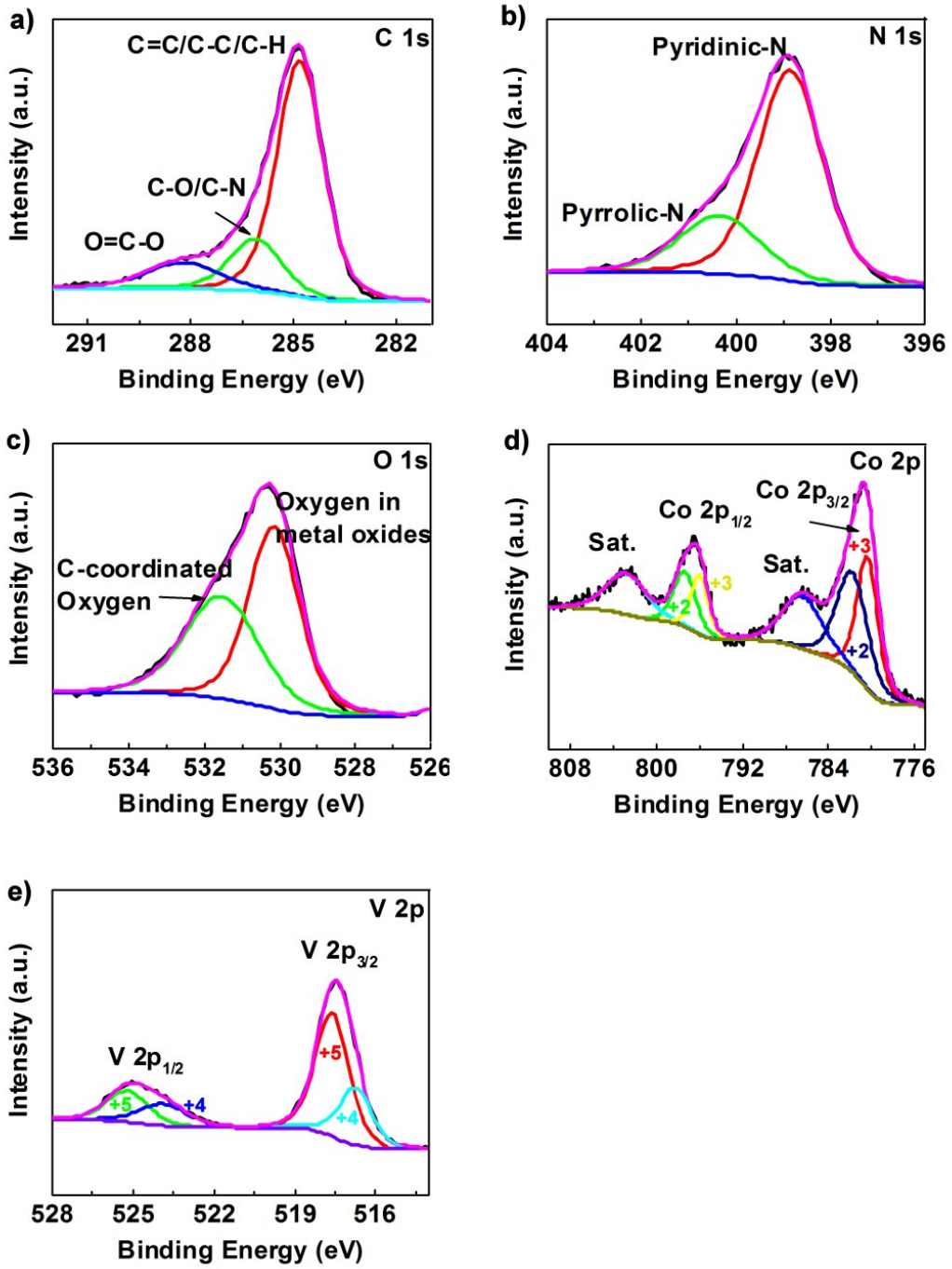

Figure S5. XPS deconvoluted spectra of **CoVO/C**, a) C 1s, b) N 1s, c) O 1s, d) Co 2p and e) V 2p.

Table S1. CHN elemental analysis of pristine ZIF-67 and **{V_{10}}@ZIF-67**

	ZIF-67 (wt.-%)	**{V_{10}}@ZIF-67 (wt.-%)**
C	37.59	33.63
H	4.23	4.75
N	21.32	18.90

Table S2. XPS elemental composition of **CoVO/C**

	atom-%	**wt.-%**
C 1s	51.3	33.8
N 1s	11.3	8.7
O 1s	25.9	22.7
V 2p	5.3	14.8
Co 2p	6.2	20.0

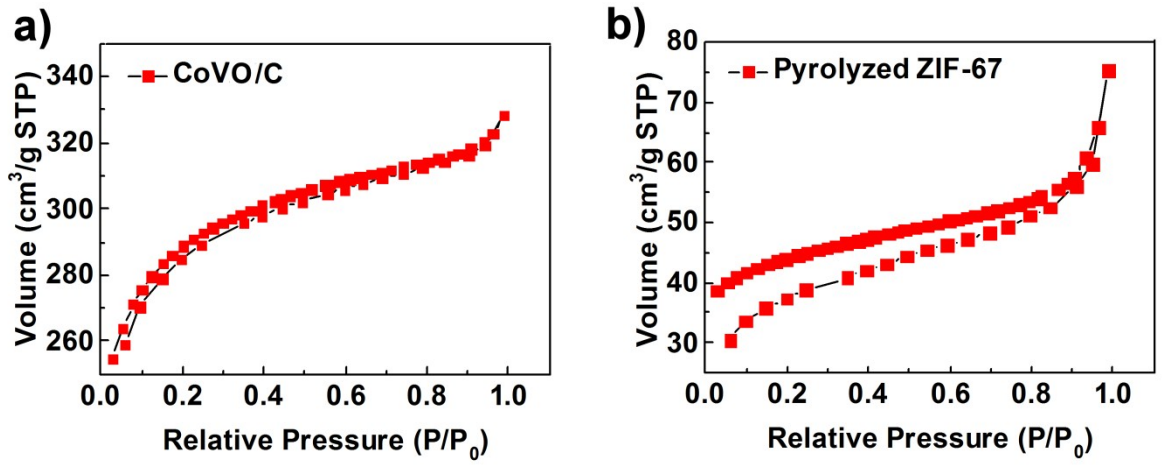

Figure S6 a) Nitrogen-sorption isotherm at 77 K of **CoVO/C**; b) Nitrogen-sorption isotherm at 77 K of ZIF-67 pyrolyzed at 480 °C.

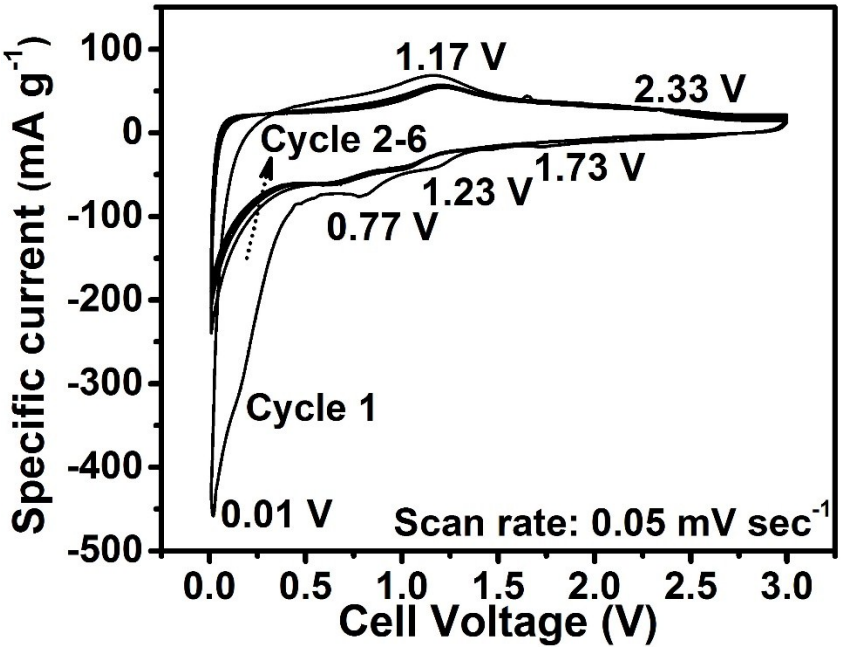

Figure S7. CV showing the first six cycles of **CoVO/C**-based electrode between 0.01 V and 3.0 V (scan rate: 0.05 mV s^{-1}).

Cyclic voltammetry (CV) curves of the first six cycles are shown in Figure S7. In the first cathodic sweep, a minor peak centered at *ca*. 1.73 V is observed which has previously been assigned to the Li^+ insertion in CoV_3O_8.[4] Further, two peaks at *ca*. 1.23 and 0.77 V are observed, which have previously been attributed to the transformation of $Co_3V_2O_8$ to CoO and $Li_yV_2O_5$, respectively.[5,6] The peak below 0.4 V is generally ascribed to the decomposition reaction of CoO to metallic Co and Li_2O, and the Li-ion insertion into the carbon, as well as the formation of the solid-electrolyte interphase (SEI) layer.[6–8] During the anodic scan, an oxidation peak is observed at *ca*. 1.17 V, indicating the extraction of Li^+ from $Li_xV_3O_7$ and $Li_yV_2O_5$ and the conversion of metallic Co to CoO.[4,5] Furthermore, a broader peak at around 2.33 V could be associated with the extraction of Li^+ from $Li_yV_2O_5$.[5] In the following cycling, only three distinct peaks at 1.1, 0.6 and < 0.3 V are observed, which are assigned to multi-step lithiation processes. In operando spectroscopic analyses are underway to gain more detailed insight into the active phases formed during electrochemical cycling.

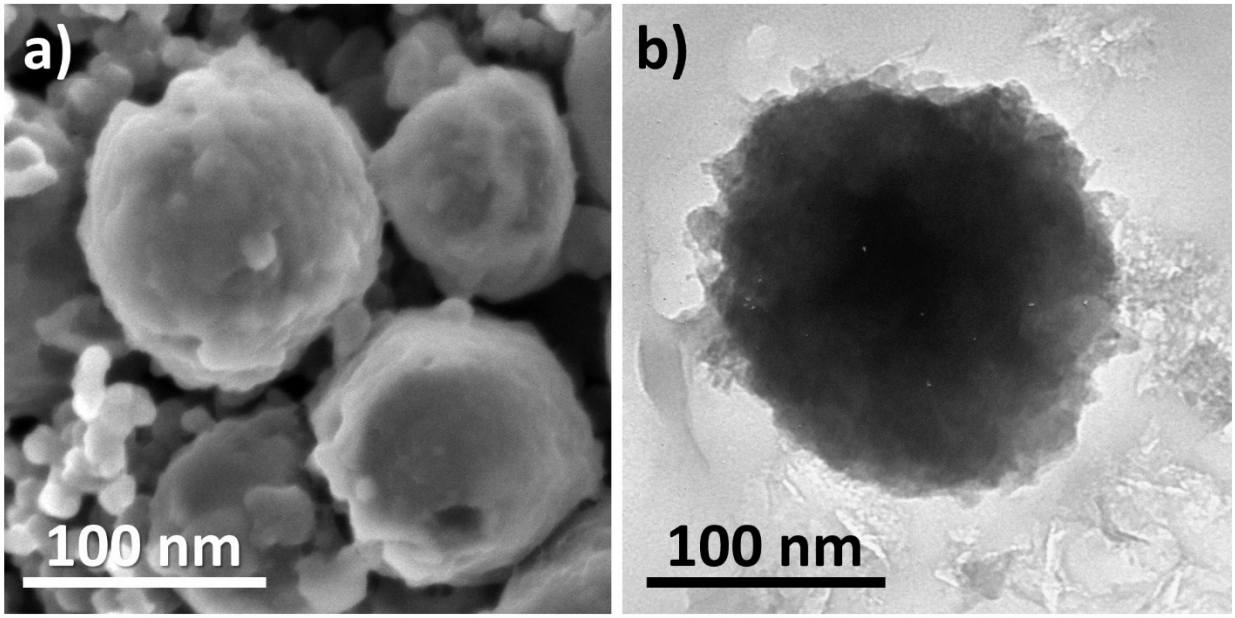

Figure S8. Ex situ (a) SEM and (b) TEM micrographs of **CoVO/C** after cycling (100 (dis-)charge cycles at 200 mA g^{-1} vs. lithium metal).

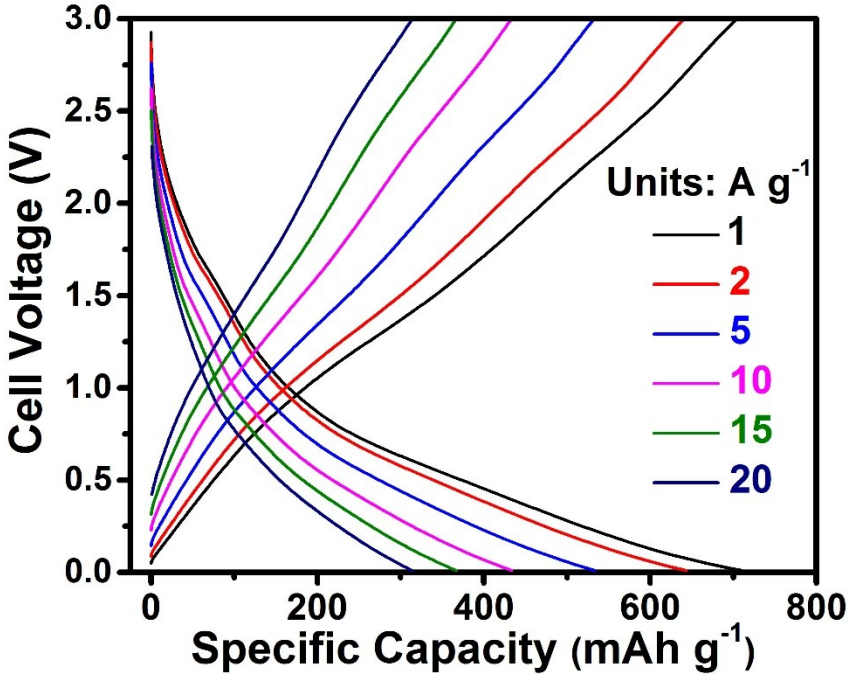

Figure S9. Potential profiles of **CoVO/C** at various current densities based on the rate capability test (Figure 2c, main text).

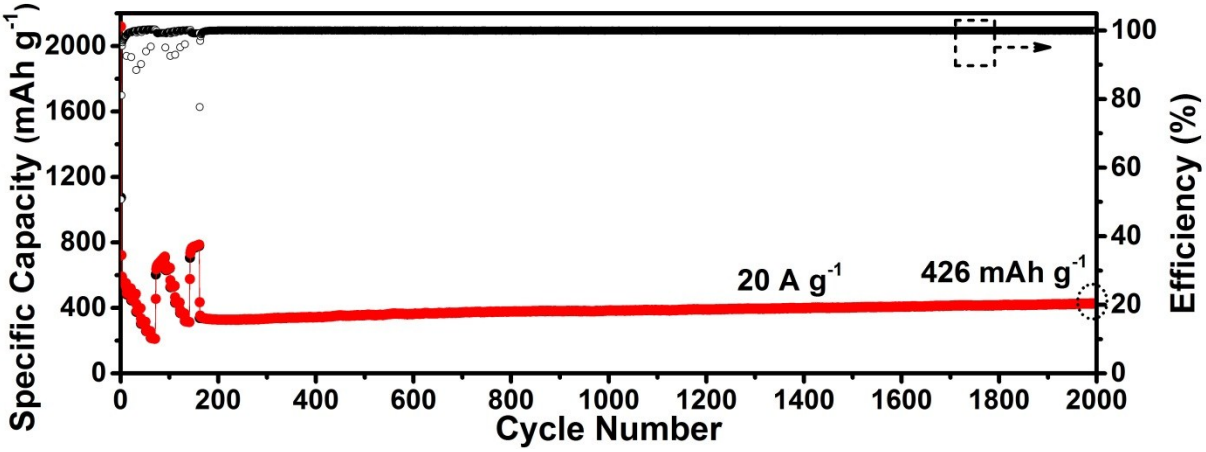

Figure S10. Rate capability test for **CoVO/C** anodes at various current rates (cycle 1 – 160) and long cycling galvanostatic measurement for **CoVO/C** anodes (cycle 161 - 2000).

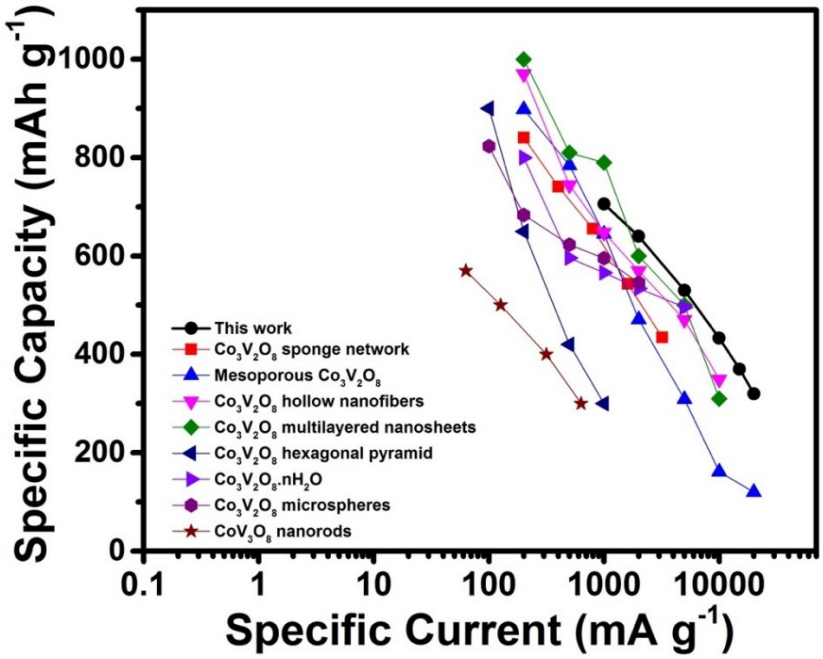

Figure S11. Comparison of Li-ion storage rate capability of **CoVO/C** and related literature systems: $Co_3V_2O_8$ sponge network,[9] mesoporous $Co_3V_2O_8$ nanoparticles,[10] $Co_3V_2O_8$ hollow nanofibers,[11] $Co_3V_2O_8$ multilayered nanosheets,[6] $Co_3V_2O_8$ hexagonal pyramid,[12] $Co_3V_2O_8 \cdot nH_2O$,[5] $Co_3V_2O_8$ microspheres,[13] CoV_3O_8 nanorods.[4]

Table S3. Comparison of the battery performance of the different POM-based and cobalt vanadate-based LIB anode materials

Materials	RC (mAh g^{-1}) / maximum CD (mA g^{-1})	RC (mAh g^{-1})/ CD (mA g^{-1})	AMR (wt.%)	Ref.
CoVO/C	510/10,000 426/20,000	920/200	80	This work
$[SiMo_{12}]$/MOF	370/1,000	570/100	70	14
$[PMo^{V}_{8}Mo^{IV}_{4}Zn_{4}]$-based POMOF	250/1,000	600/100	70	15
$[PW_{12}Cu_{10}]$/MCF	298/1,000	553/100	70	16
$[PMo_{12}V_{2}]$-ILs@MOFs	348/3,000	930/200	70	17
$Co_2V_2O_7$ microplatelets	344/5,000	813/200	70	18
$Co_3V_2O_8$ nH_2O	496/5,000	800/200	70	5
$Co_3V_2O_8$ nanosheets	300/10,000	880/200	70	6
Co_3O_4@$Co_3V_2O_8$	578/5,000	916/200	70	19
$[PW_9Ni_6]$-based MOF	NA	350/400	65	20
$[PMo_{12}V_2]$-based MOF/rGO	428/2,000	846/200	70	21

POMOF: POM-based metal organic frameworks;

MCF: metal-carbene frameworks;

RC: Reversible capacity;

AMR: Active material ratio;

CD: Current density.

Table S4. Comparison of the OER performance of literature-known POM-MOF-based noble-metal-free catalysts

Catalyst	Loading density (mg/cm^2)	Onset potential (V)	Overpotential (mV) at 10 mA cm^{-2}	Tafel slope (mV dec^{-1})	Ref.
CoVO/C	0.3	1.5	350	75	**This work**
POM@ZIF-8	~0.6	--	784 (at 1 mA cm^{-2}, neutral pH)	784	22
Mo_xCo_xC particles	~0.7	1.5	295	35	23
$Co_3O_4/CoMoO_4$	~0.25	1.47	318	63	24
NiCoP/C	~0.25	1.48	330	96	25
$Co_3O_4/NiCo_2O_4$ cages	1.0	1.53	340	88	26
Co_3ZnC/Co@CN	~0.34	1.5	366	81	27
NCNTFs	0.2	1.47	370	93	28
Ni-Co mixed oxide cages	--	1.56	380	50	29
Co@NCNT	~0.42	1.58	429	116	30
$CoMoO_4$	~0.24	1.6	410	84	31
Co_3O_4	~0.14	1.52	400	72	32
CoV_2O_6-V_2O_5/NRGO-1	~0.14	--	239	50	33

References:

1 I. Omri, T. Mhiri and M. Graia, *J. Mol. Struct.*, 2015, **1098**, 324–331.

2 P. Román, A. Aranzabe, A. Luque, J. M. Gutiérrez-Zorrilla and M. Martínez-Ripoll, *J. Chem. Soc. Dalt. Trans.*, 1995, **0**, 2225–2231.

3 G. C. Ou, L. Jiang, X. L. Feng and T. B. Lu, *Dalt. Trans.*, 2009, **0**, 71–76.

4 G. H. Jeong, I. Lee, D. Lee, H.-M. Lee, S. Baek, O.-P. Kwon, P. N. Kumta, S. Yoon and S.-W. Kim, *Nanotechnology*, 2018, **29**, 195403.

5 F. Wu, S. Xiong, Y. Qian and S.-H. Yu, *Angew. Chemie Int. Ed.*, 2015, **54**, 10787–10791.

6 G. Yang, H. Cui, G. Yang and C. Wang, *ACS Nano*, 2014, **8**, 4474–4487.

7 Y. Luo, X. Xu, X. Tian, Q. Wei, M. Yan, K. Zhao, X. Xu and L. Mai, *J. Mater. Chem. A*, 2016, **4**, 5075–5080.

8 Y. Ma, Y. Ma, D. Geiger, U. Kaiser, H. Zhang, G. T. Kim, T. Diemant, R. J. Behm, A. Varzi and S. Passerini, *Nano Energy*, 2017, **42**, 341–352.

9 V. Soundharrajan, B. Sambandam, J. Song, S. Kim, J. Jo, S. Kim, S. Lee, V. Mathew and J. Kim, *ACS Appl. Mater. Interfaces*, 2016, **8**, 8546–8553.

10 G. Gao, S. Lu, B. Dong, Y. Xiang, K. Xi and S. Ding, *J. Mater. Chem. A*, 2016, **4**, 6264–6270.

11 J. Xiang, X.-Y. Yu and U. Paik, *J. Power Sources*, 2016, **329**, 190–196.

12 Q. Zhang, J. Pei, G. Chen, C. Bie, D. Chen, Y. Jiao and J. Rao, *Electrochim. Acta*, 2017, **238**, 227–236.

13 H. Chai, Y. Wang, Y. Fang, Y. Lv, H. Dong, D. Jia and W. Zhou, *Chem. Eng. J.*, 2017, **326**, 587–593.

14 X.-Y. Yang, T. Wei, J.-S. Li, N. Sheng, P.-P. Zhu, J.-Q. Sha, T. Wang and Y.-Q. Lan, *Inorg. Chem.*, 2017, **56**, 8311–8318.

15 Q. Huang, T. Wei, M. Zhang, L.-Z. Dong, A.-M. Zhang, S.-L. Li, W.-J. Liu, J. Liu and Y.-Q. Lan, *J. Mater. Chem. A*, 2017, **5**, 8477–8483.

16 P.-P. Zhu, N. Sheng, M.-T. Li, J.-S. Li, G.-D. Liu, X.-Y. Yang, J.-Q. Sha, M.-L. Zhu and J. Jiang, *J. Mater. Chem. A*, 2017, **5**, 17920–17925.

17 M. Zhang, A. M. Zhang, X. X. Wang, Q. Huang, X. Zhu, X. L. Wang, L. Z. Dong, S. L. Li and Y. Q. Lan, *J. Mater. Chem. A*, 2018, **6**, 8735–8741.

18 F. Wu, C. Yu, W. Liu, T. Wang, J. Feng and S. Xiong, *J. Mater. Chem. A*, 2015, **3**, 16728–16736.

19 Y. Lu, L. Yu, M. Wu, Y. Wang and X. W. D. Lou, *Adv. Mater.*, 2018, **30**, 1702875.

20 Y. Yue, Y. Li, Z. Bi, G. M. Veith, C. A. Bridges, B. Guo, J. Chen, D. R. Mullins, S. P. Surwade, S. M. Mahurin, H. Liu, M. P. Paranthaman and S. Dai, *J. Mater. Chem. A*, 2015, **3**, 22989–22995.

21 T. Wei, M. Zhang, P. Wu, Y. Tang, S. Li, F. Shen and X. Wang, *Nano Energy*, 2017, **34**, 205–214.

22 S. Mukhopadhyay, J. Debgupta, C. Singh, A. Kar and S. K. Das, *Angew. Chemie - Int. Ed.*, 2018, **57**, 1918–1923.

23 C. Chen, A. Wu, H. Yan, Y. Xiao, C. Tian and H. Fu, *Chem. Sci.*, 2018, **9**, 4746–4755.

24 L. Zhang, T. Mi, M. A. Ziaee, L. Liang and R. Wang, *J. Mater. Chem. A*, 2018, **6**, 1639–1647.

25 P. He, X. Y. Yu and X. W. D. Lou, *Angew. Chemie - Int. Ed.*, 2017, **56**, 3897–3900.

26 H. Hu, B. Guan, B. Xia and X. W. Lou, *J. Am. Chem. Soc.*, 2015, **137**, 5590–5595.

27 J. Su, G. Xia, R. Li, Y. Yang, J. Chen, R. Shi, P. Jiang and Q. Chen, *J. Mater. Chem. A*, 2016, **4**, 9204–9212.

28 B. Y. Xia, Y. Yan, N. Li, H. Bin Wu, X. W. D. Lou and X. Wang, *Nat. Energy*, 2016, **1**, 15006.

29 L. Han, X. Y. Yu and X. W. (David) Lou, *Adv. Mater.*, 2016, **28**, 4601–4605.

30 E. Zhang, Y. Xie, S. Ci, J. Jia, P. Cai, L. Yi and Z. Wen, *J. Mater. Chem. A*, 2016, **4**, 17288–17298.

31 Y. Yang, S. Wang, C. Jiang, Q. Lu, Z. Tang and X. Wang, *Chem. Mater.*, 2016, **28**, 2417–2423.

32 Y. Wang, T. Zhou, K. Jiang, P. Da, Z. Peng, J. Tang, B. Kong, W. Bin Cai, Z. Yang and G. Zheng, *Adv. Energy Mater.*, 2014, **4**, 1400696.

33 F.-C. Shen, Y. Wang, Y.-J. Tang, S.-L. Li, Y.-R. Wang, L.-Z. Dong, Y.-F. Li, A. Yan Xu and Y.-Q. Lan, *ACS Energy Lett.*, 2017, **2**, 1327–1333.